Supporting Information

Designing Ferrimagnetic-Ferroelastic Multiferroic Semiconductor in $FeMoClO_4$ Nanosheet via Element Substitution

Lijuan Yan,[a] Xiaofeng Liu,[b,c,d] Pengfei Gao,[e] Xiangyang Li,[*b] and Xingxing Li[*b,c]

[a]College of Electronics & Information Engineering, Guangdong Ocean University, Zhanjian, Guangdong 524088, China

[b]Hefei National Research Center for Physical Sciences at the Microscale, University of Science and Technology of China, Hefei, Anhui 230026, China

[c]Department of Chemical Physics, University of Science and Technology of China, Hefei, Anhui 230026, China

[d]School of Physics, Hefei University of Technology, Hefei, Anhui 230009, China

[e]Interdisciplinary Center for Fundamental and Frontier Sciences, Nanjing University of Science and Technology, Jiangyin, Jiangsu 214443, China

*E-mail: xyangli@ustc.edu.cn

*E-mail: lixx@ustc.edu.cn

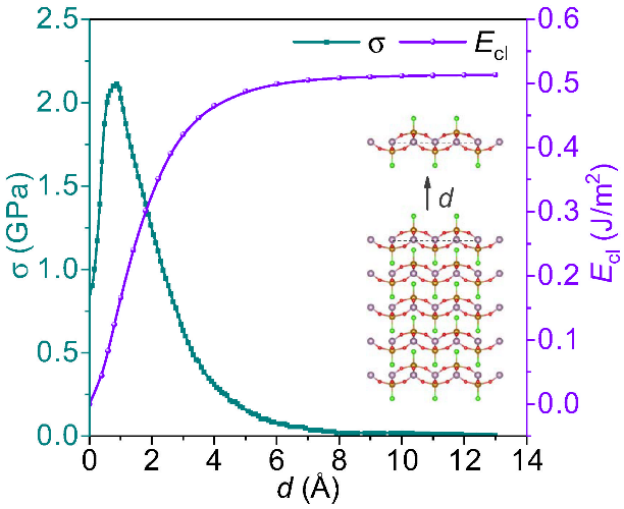

Figure S1. Exfoliation energy E_{cl} and cleavage strength σ as functions of separation distance d in the process of exfoliating one nanosheet from its bulk crystal.

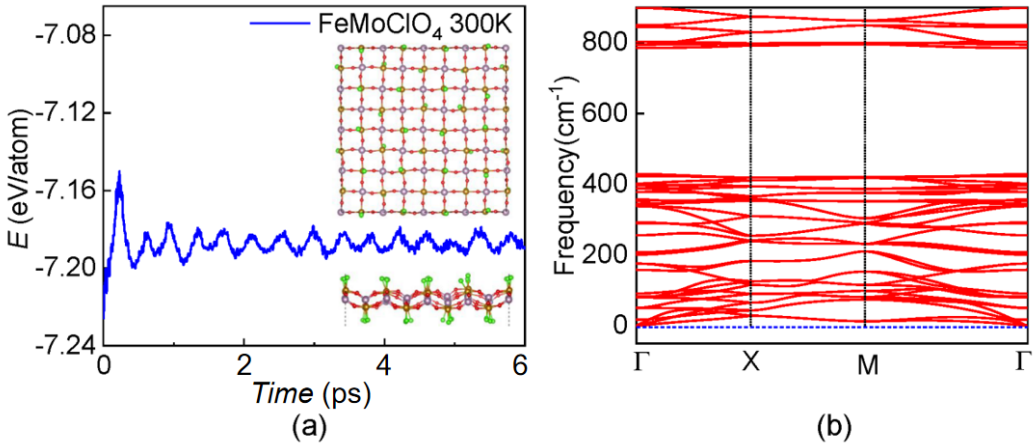

Figure S2. (a) *Ab initio* molecular dynamics (AIMD) simulation of total energy with time for $FeMoClO_4$ with a P4/nmm space group at 300 K. The insets depict snapshots of 4×4×1 supercell containing 224 atoms after 6 *ps*. (b) Phonon dispersions of the $FeMoClO_4$ nanosheet.

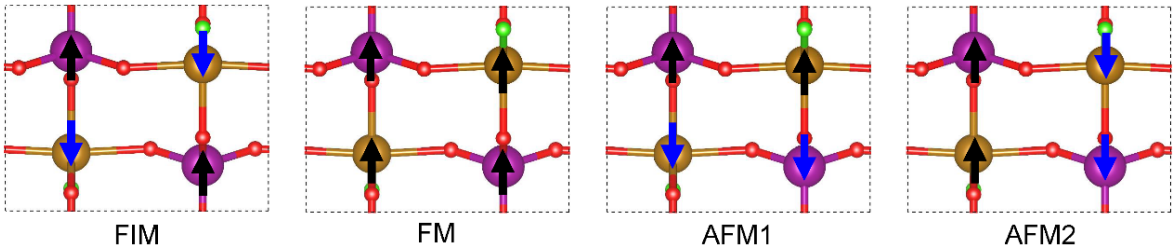

Figure S3. Four different magnetic states calculated for $FeMnClO_4$ nanosheet. They contain one ferrimagnetic (FIM) state, one ferromagnetic (FM) state, and two antiferromagnetic (AFM) states.

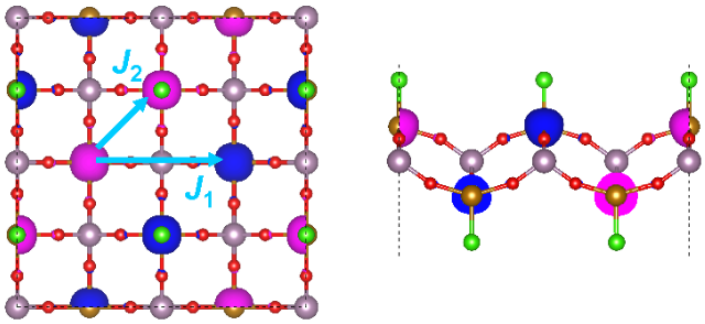

Figure S4. Spin density, nearest and next-nearest spin exchange (J_1 and J_2) paths for the $FeMoClO_4$ nanosheet. Pink (Blue) denotes spin-up (spin-down) component.

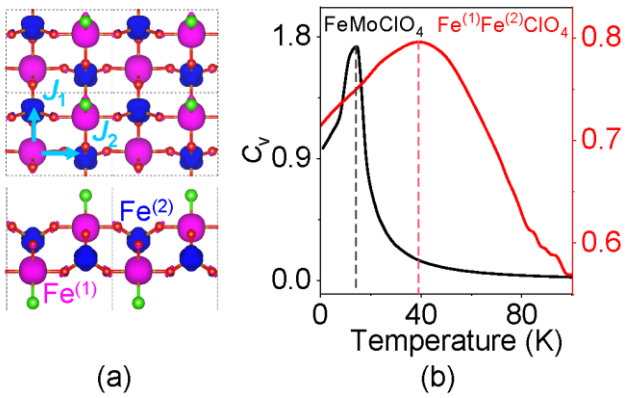

Figure S5. (a) Spin density, nearest and next-nearest spin exchange (J_1 and J_2) paths for 2D $Fe^{(1)}Fe^{(2)}ClO_4$. Pink (Blue) denotes spin-up (spin-down) component. The specific values of spin exchange parameters are shown in Table S4. After $Fe^{(2)6+}$ replaces Mo^{6+}, the calculated magnetic moment of $Fe^{(1)}Fe^{(2)}ClO_4$ is 6 μ_B per unit cell, which is 2 μ_B per unit cell lower than that of $FeMnClO_4$. Noted that among the entire 3d transition metals, Mo^{6+} can be substituted by Cr^{6+} besides Fe^{6+} and Mn^{6+}, but $FeCrClO_4$ has an AFM ground state as well as $FeMoClO_4$. Other transition metals that can not possess a +6 charge state are discarded. (b) Specific heat (C_v) as a function of temperature for $FeMoClO_4$ and $Fe^{(1)}Fe^{(2)}ClO_4$. The calculated Curie temperature (T_c = 39 K) of $Fe^{(1)}Fe^{(2)}ClO_4$ is higher than 14 K of $FeMoClO_4$, but lower than 127 K of $FeMnClO_4$.

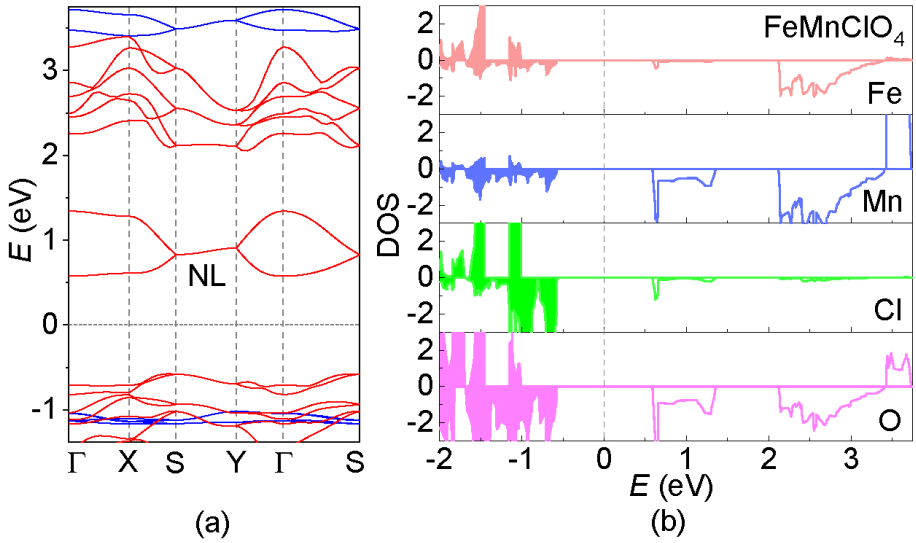

Figure S6. (a) Spin-polarized band structure and (b) projected density of states for the $FeMnClO_4$ nanosheet calculated by HSE06 functional.

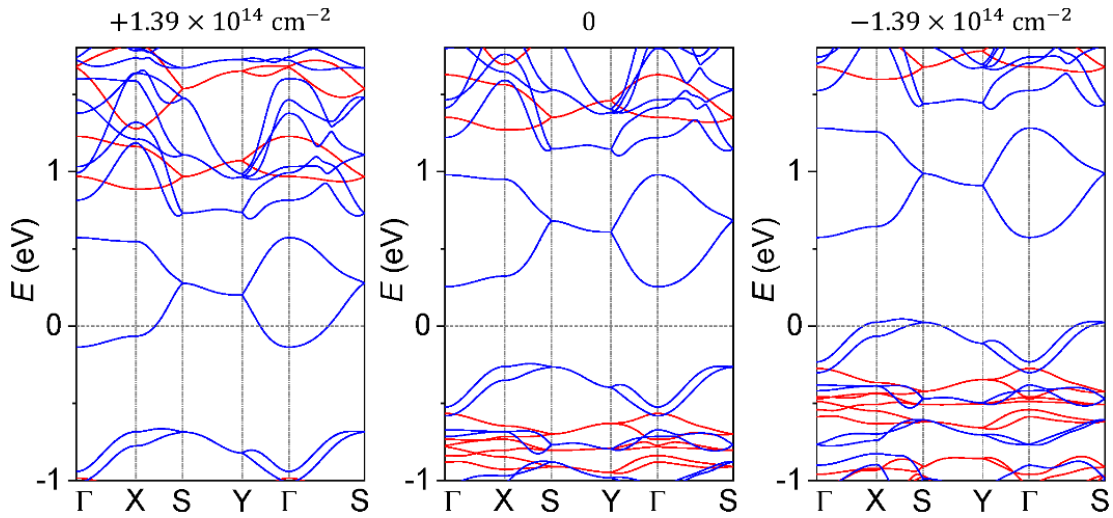

Figure S7. Band structure of $FeMnClO_4$ nanosheet for electron doping (left), pure (middle) and hole doping (right) with a carrier concentration of ± 1.39 × 10^{14} cm^{-2}. Positive and negative values above the panel represent electron and hole doping, respectively.

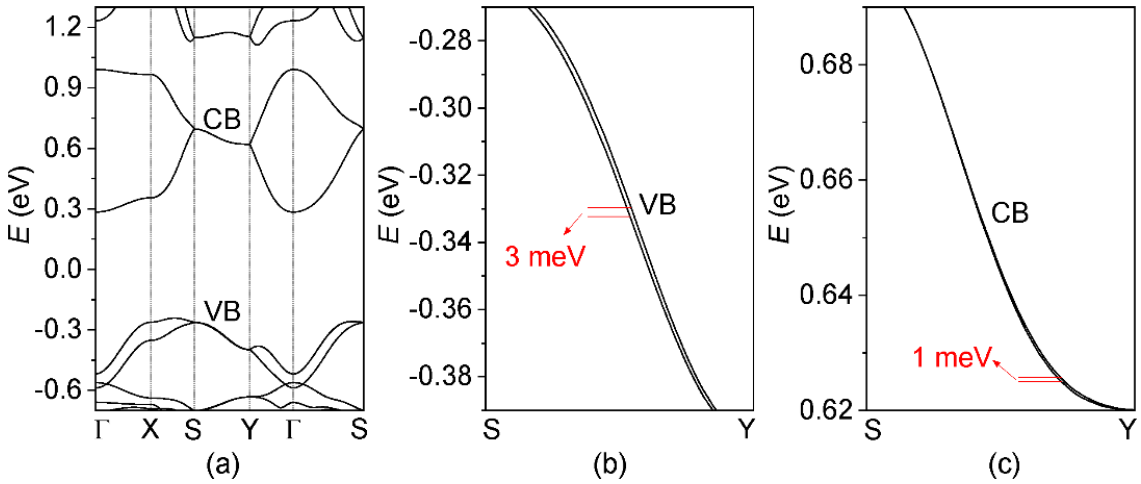

Figure S8. (a) Band structure of $FeMnClO_4$ nanosheet after considering the spin orbit coupling effect. (b, c) Topological nodal lines in valence band (VB) and conduction band (CB).

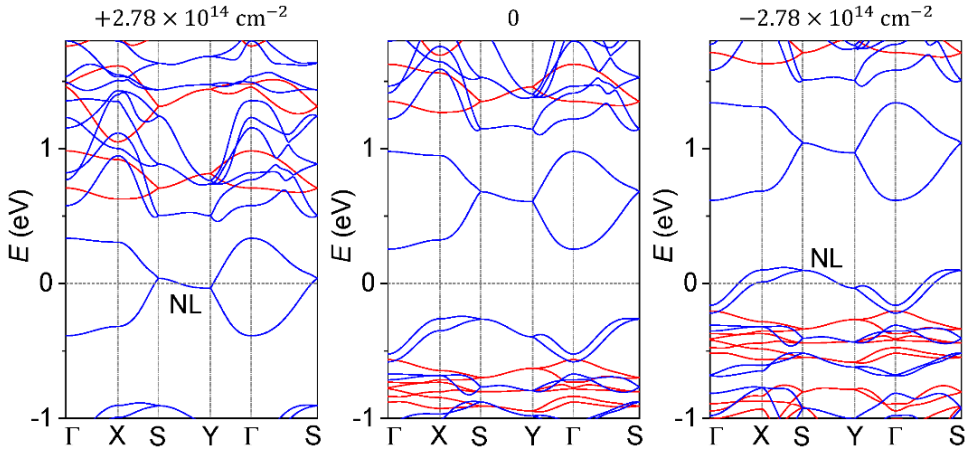

Figure S9. Band structure of $FeMnClO_4$ nanosheet for electron doping (left), pure (middle) and hole doping (right) with a carrier concentration of 2.78×10^{14} cm^{-2}. Positive and negative values above the panel represent electron and hole doping, respectively.

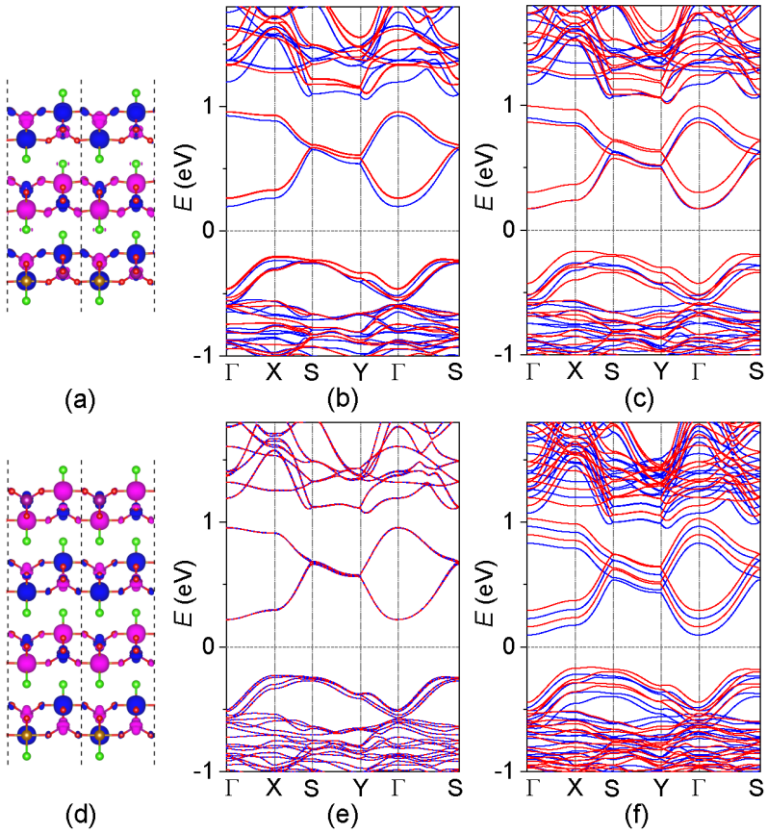

Figure S10. (a, d) Spin densities and (b, c, e, f) band structures of trilayer and four-layer $FeMnClO_4$, where the band structures in (c, f) panels are plotted under a perpendicular electric field of 0.01 V/Å.

Table S1. Calculated relative energies of ferromagnetic (FM) state to ferrimagnetic (FIM) state ΔE (eV per chemical formula) for $FeMnClO_4$ at different values of onsite Coulomb interaction U.

ΔE ($FeMnClO_4$)	U_{Mn}=2	U_{Mn}=3	U_{Mn}=4	U_{Mn}=5	U_{Mn}=6
U_{Fe}=2	0.726	0.677	0.607	0.512	0.376
U_{Fe}=3	0.696	0.656	0.588	0.495	0.394
U_{Fe}=4	0.659	0.627	0.556	0.474	0.387
U_{Fe}=5	0.621	0.593	0.523	0.451	0.374
U_{Fe}=6	0.581	0.552	0.488	0.424	0.357

Table S2. Magnetic exchange parameters (in meV), magnetic anisotropy energies (meV per chemical formula), and axial (planar) anisotropy strength (meV) for the $FeMoClO_4$ nanosheet.

$FeMoClO_4$	J_1	J_2	$E_{[010]}$-$E_{[100]}$	$E_{[001]}$-$E_{[100]}$	D_{Fe}	E_{Fe}
	0.23	0.14	0	1.32	0.21	0.00

Table S3. Magnetic exchange parameters (in meV), magnetic anisotropy energies (meV per chemical formula), and axial (planar) anisotropy strength (meV) for the $FeMnClO_4$ nanosheet.

$FeMnClO_4$	J_1	J_2	$E_{[010]}$-$E_{[100]}$	$E_{[001]}$-$E_{[100]}$	D_{Fe}	E_{Fe}	D_{Mn}	E_{Mn}
	45.77	13.00	0.61	1.31	0.13	0.03	0.38	0.59

Table S4. Magnetic exchange parameters (in meV), magnetic anisotropy energies (meV per chemical formula), and axial (planar) anisotropy strength (meV) for the $Fe^{(1)}Fe^{(2)}ClO_4$ nanosheet.

$Fe^{(1)}Fe^{(2)}ClO_4$	J_1	J_2	$E_{[010]}$-$E_{[100]}$	$E_{[001]}$-$E_{[100]}$	$D_{Fe(1)}$	$E_{Fe(1)}$	$D_{Fe(2)}$	$E_{Fe(2)}$
	18.47	1.98	0.48	1.21	0.10	0.01	-0.14	0.06